

Vortex nucleation in rotating Bose-Einstein condensates with density-dependent gauge potential

Ishfaq Ahmad Bhat¹, Thudiyangal Mithun², Bishwajyoti Dey¹

¹ *Department of Physics, Savitribai Phule Pune University, Pune, Maharashtra, India, 411007*

² *Department of Mathematics and Statistics, University of Massachusetts, Amherst Massachusetts 01003-4515, USA*

We study numerically the vortex dynamics and vortex-lattice formation in a rotating density-dependent Bose-Einstein condensate (BEC), characterized by the presence of nonlinear rotation. By varying the strength of nonlinear rotation in density-dependent BECs, we calculate the critical frequency, Ω_{cr} , for vortex nucleation both in adiabatic and sudden external trap rotations. The nonlinear rotation modifies the extent of deformation experienced by the BEC due to the trap and shifts the Ω_{cr} values for vortex nucleation. The critical frequencies and thereby, the transition to vortex-lattices in an adiabatic rotation ramp, depend on conventional s -wave scattering lengths through the strength of nonlinear rotation, C , such that $\Omega_{\text{cr}}(C > 0) < \Omega_{\text{cr}}(C = 0) < \Omega_{\text{cr}}(C < 0)$. In an analogous manner, the critical ellipticity (ϵ_{cr}) for vortex nucleation during an adiabatic introduction of trap ellipticity (ϵ) depends on the nature of nonlinear rotation besides trap rotation frequency. The nonlinear rotation additionally affects the vortex-vortex interactions and the motion of the vortices through the condensate by altering the strength of Magnus force on them. The combined result of these nonlinear effects is the formation of the non-Abrikosov vortex-lattices and ring-vortex arrangements in the density-dependent BECs.

PACS numbers:

I. INTRODUCTION:

Soon after the successful realization of Bose-Einstein condensates (BECs) in alkali metal atoms, the study of quantized vortices and their dynamics in them gained an active interest [1–7]. Quantum vortices in BECs and superfluid ^4He [8] are the topological defects that arise in response to the external rotation [2–5], shaking a BEC [9, 10] or even moving an obstacle through the condensate [11, 12]. The rotation in a BEC is induced by stirring the atomic cloud and can be either adiabatic or sudden (nonadiabatic). In either case the nucleation of vortices within the condensate occurs only when the trap rotation exceeds a certain minimum value called critical frequency, Ω_{cr} . At this stage the vortices in BEC become energetically favorable. For rotational frequencies greater than Ω_{cr} , multiple vortices enter the condensate and eventually form a vortex-lattice. In nonadiabatic rotations, the critical rotation frequency, Ω_{cr} , at which a single vortex exists stably at the minimum of the trap, decreases with the increasing strength of two- [13–15] and three-body [16] interaction strengths. The change in Ω_{cr} is, however, marginal at large interaction strengths and $\Omega_{\text{cr}} \simeq 0.65\omega_{\perp}$, where ω_{\perp} is the transverse trapping frequency, for the creation of single vortex in the ENS experiment [17]. On the other hand, in an adiabatic rotation ramp for a fixed trap ellipticity, conventional BECs with only short range s -wave interactions form vortex lattices when the trap rotation frequencies are $\approx \omega_{\perp}/\sqrt{2}$ [2–4]. This transition from the vortex free state to the vortex-lattice structure occurs via dynamical instability [3, 7] and is independent of the s -wave interaction strength and longitudinal confinement. Likewise, vortex-lattices are also achieved by varying ϵ in a linear fashion at fixed trap rotation [3, 18]. Here the transition to the vortex-

lattice structure is characterized by the critical ellipticity, ϵ_{cr} , depending only on the trap rotation frequency. Long range dipole-dipole interactions and trap geometry within the dipolar BECs are, however, found to alter these critical frequencies and ellipticities [19–23].

In addition to providing a flexible test-bed for numerous quantum phenomena, BECs are even noted for the experimental realization of artificial electromagnetism in them [24, 25]. This has been made possible through the engineering of artificial gauge potentials in these ultracold condensates. Induced electromagnetism in BECs has led to the emergence of novel phenomena like density-dependent magnetism [26], exotic spin-orbit [27] and spin angular momentum couplings [28, 29]. However, the nature of gauge potentials in BECs is typically static with no feedback between light and matter waves. In dynamical gauge fields, on the other hand, nonlinear feedback between matter and gauge fields plays a role. This back-action is expected to enrich the physics of atomic and nonlinear systems and has been realized in experiments recently [30, 31].

Scalar and nonrotating BECs with density-dependent gauge potentials, known as *Chiral* condensates, have been already studied in one-dimension for anyonic structures [32], chiral solitons [33–36] and collective excitations [37] in them. More recently, strong density-dependent gauge potentials are even shown to realize chaotic collective dynamics in two-dimensional BECs [38]. The response of density-dependent BECs against the trap rotation in two-dimensions has been studied in Refs. [39, 40] where vortex ground states have been simulated numerically. The density-dependent gauge potential realizes an effective nonlinear rotation in BECs, thereby leading to non-Abrikosov vortex-lattices and ring vortex arrangements. In contrast to the Abrikosov

vortex-lattices in scalar BECs [41–43], the non-Abrikosov vortex-lattices in BECs with density-dependent gauge potentials lack the hexagonal (or triangular) symmetry in the vortex arrangements [39, 40].

The present paper studies the effects of nonlinear rotation on the dynamics of vortex lattice formation in these BECs within the scope of time-dependent numerical simulations. The studies of vortex nucleation in conventional [2, 3, 7, 44, 45] and dipolar [21–23] BECs reveal that the transition to the vortex-lattices in an adiabatic rotation ramp depends only on the rotation frequency and trap ellipticity but is independent of the s -wave interaction strength. Here we show that unlike in conventional and dipolar condensates, this transition depends on the short range s -wave interactions in density-dependent condensates. The density-dependent BECs show similar responses against the adiabatic and sudden rotations such that the number and arrangement of the nucleated vortices varies with the strength of the nonlinear rotations. In addition to the energy considerations, the non-Abrikosov vortex-lattices and ring-vortex arrangements in these condensates are a result of the modifications in the Magnus force experienced by the vortices and the repulsive interactions between them.

The subsequent material is structured as follows. In Sec. II we introduce the model in the form of Gross-Pitaevskii equation including the density-dependent gauge potential. This is followed by Sec. III where we present the possible routes to vortex nucleation through numerical investigations based on the Crank Nicholson method. The work is finally summarized in Sec. IV.

II. MODEL

We consider a weakly interacting BEC of N two-level atoms coupled by a coherent light-matter interaction due to an applied laser field. Within the rotating-wave approximation, such a BEC is described by the following mean-field Hamiltonian [24, 39, 46]:

$$\hat{\mathcal{H}} = \left(\frac{\hat{\mathbf{p}}^2}{2m} + V(\mathbf{r}) \right) \otimes \mathbb{1} + \hat{\mathcal{H}}_{\text{int}} + \hat{\mathcal{U}}_{\text{MF}} \quad (1)$$

where in the first term $\hat{\mathbf{p}}$ is the momentum operator, $V(\mathbf{r}) = m(\omega_x^2 x^2 + \omega_y^2 y^2 + \omega_z^2 z^2)/2$ is the trapping potential and $\mathbb{1}$ symbolizes the 2×2 unity matrix. The mean-field interactions, $\hat{\mathcal{H}}_{\text{int}} = (1/2)\text{diag}[\Delta_1, \Delta_2]$ with $\Delta_i = g_{ii}|\Psi_i|^2 + g_{ij}|\Psi_j|^2$ and $g_{ij} = 4\pi\hbar^2 a_{ij}/m$ where a_{ij} are the respective scattering lengths of the collisions between atoms in internal states i and j ($i, j = 1, 2$). Further, the light-matter interactions accounted by Refs. [25, 46],

$$\hat{\mathcal{U}}_{\text{MF}} = \frac{\hbar\Omega_r}{2} \begin{pmatrix} \cos\theta(\mathbf{r}) & e^{-i\phi(\mathbf{r})}\sin\theta(\mathbf{r}) \\ e^{i\phi(\mathbf{r})}\sin\theta(\mathbf{r}) & -\cos\theta(\mathbf{r}) \end{pmatrix} \quad (2)$$

are parameterized in terms of Rabi frequency, Ω_r , mixing angle, $\theta(\mathbf{r})$ and phase of the incident laser beam, $\phi(\mathbf{r})$. We use perturbation theory by defining the perturbed

states in terms of the unperturbed eigen-states $|\pm\rangle$ of $\hat{\mathcal{U}}_{\text{MF}}$ [39, 40, 46]:

$$|\Psi_{\pm}\rangle = |\pm\rangle \pm \frac{\Delta_d}{\hbar\Omega_r} |\mp\rangle \quad (3)$$

where $\Delta_d = \sin(\theta/2)\cos(\theta/2)(\Delta_1 - \Delta_2)/2$ is the mean-field detuning. Since the qualitative details do not depend on which of the two perturbed states is chosen, therefore, we chose the Ψ_+ -state and write the effective Hamiltonian as [39, 40, 46]:

$$\hat{H}_+ = \frac{(\hat{\mathbf{p}} - \mathbf{A}_+)^2}{2m} + W_+ + \frac{\hbar\Omega_r}{2} + \Delta_+ + V(\mathbf{r}), \quad (4)$$

where the vector gauge potential is defined as, $\mathbf{A}_+ = i\hbar\langle\Psi_+|\nabla|\Psi_+\rangle$, while the scalar potential, $W_+ = \hbar^2|\langle\Psi_+|\nabla\Psi_+\rangle|^2/2m$ and $\Delta_+ = (\Delta_1\cos^2(\theta/2) + \Delta_2\sin^2(\theta/2))/2$ is the dressed mean-field interaction. The generalized mean-field Gross-Pitaevskii (GP) equation for Ψ_+ is finally obtained by extremizing the energy functional, $\mathcal{E} = \langle\Psi_+|\hat{H}_+|\Psi_+\rangle$ as [39, 46–48]:

$$i\hbar\frac{\partial\Psi_+}{\partial t} = \left[\frac{(\hat{\mathbf{p}} - \mathbf{A}_+)^2}{2m} + \mathbf{a}_1 \cdot \mathbf{J} \right] \Psi_+ + \left[V(\mathbf{r}) + \frac{\hbar\Omega_r}{2} + 2\Delta_+ + W_+ \right] \Psi_+ + \left[\mathbf{n}_+ \left(\frac{\partial W_+}{\partial\Psi_+^*} - \nabla \cdot \frac{\partial W_+}{\partial\nabla\Psi_+^*} \right) - \frac{\partial W_+}{\partial\nabla\Psi_+^*} \cdot \nabla\mathbf{n}_+ \right] \Psi_+ \quad (5)$$

Here $\mathbf{n}_+ = |\Psi_+(\mathbf{r}, t)|^2$ is the atomic density of the BEC in the $|\Psi_+\rangle$ state, $\mathbf{a}_1 = \nabla\phi\Delta_d\sin\theta/\mathbf{n}_+\Omega_r$ is the strength of the coupling to the gauge field and

$$\mathbf{J} = \frac{\hbar}{2mi} \left[\Psi_+ \left(\nabla + \frac{i}{\hbar}\mathbf{A}_+ \right) \Psi_+^* - \Psi_+^* \left(\nabla - \frac{i}{\hbar}\mathbf{A}_+ \right) \Psi_+ \right] \quad (6)$$

is the nonlinear current. We now expand the gauge potentials \mathbf{A}_+ and W_+ to first order in small parameters $-\theta = \Omega_r/\Delta$ representing the ratio of Rabi frequency to laser detuning, and $\epsilon = \mathbf{n}_+(\mathbf{r})(g_{11} - g_{12})/4\hbar\Delta$ which takes into account the collisional and coherent interactions, to obtain the simplified relations for the potentials [39, 40]:

$$\mathbf{A}_+ = -\frac{\hbar\theta^2}{4}(1 - 4\epsilon)\nabla\phi \quad (7)$$

$$W_+ = \frac{\hbar^2}{2} \left(\frac{(\nabla\theta)^2(1 - 4\epsilon) + \theta^2(1 + 4\epsilon)(\nabla\phi)^2}{4m} - \nabla\theta^2 \cdot \nabla\epsilon \right) \quad (8)$$

We further invoke the spatial dependence in Rabi coupling through $\Omega_r = \kappa_0 r$, where r is the radial distance and κ_0 is a constant, and define the phase, $\phi = l\varphi$ where

l and φ are respectively the angular momenta and polar angle of the incident laser beam [49]. The density-dependent gauge potentials (Eqs. (7) and (8)) when substituted in Eq. (5) in a rotating frame gives the simplified three-dimensional GP equation as [39, 40]:

$$i\hbar\frac{\partial\Psi}{\partial t} = \left[-\frac{\hbar^2}{2m}\nabla^2 + V(\mathbf{r}) - \Omega_n(\mathbf{r}, t)\hat{L}_z + g_{\text{eff}}|\Psi|^2 \right] \Psi \quad (9)$$

In Eq. (9), the subscript + is omitted, the operator $\nabla^2 = \frac{\partial^2}{\partial x^2} + \frac{\partial^2}{\partial y^2} + \frac{\partial^2}{\partial z^2}$, and $\hat{L}_z = -i\hbar\left(x\frac{\partial}{\partial y} - y\frac{\partial}{\partial x}\right)$ is the z component of the angular momentum operator. The density-dependent rotation experienced by the BEC, $\Omega_n(\mathbf{r}, t)$ has the form,

$$\Omega_n(\mathbf{r}, t) = \Omega_0 + Cn(\mathbf{r}, t), \quad (10)$$

where Ω_0 represents the trap rotation and $n(\mathbf{r}, t) = |\Psi(\mathbf{r}, t)|^2$ is the number density of the BEC. The nonlinear rotation strength, $C = l\theta_0^2(g_{11} - g_{12})/(m\Delta)$ where $\theta_0 = \kappa_0/\Delta$ while the mean-field interaction, $g_{\text{eff}} = g_{11} + \hbar(2l^2 - 1)C/4l$. It is worth mentioning that the allowed values of C in a density-dependent BEC with $g_{\text{eff}} > 0$ are bounded by $\pm C_{\text{max}}$, where $C_{\text{max}} = \sqrt{8\pi(\ln 2)g_{\text{eff}}/3Nm}$ [40]. Otherwise the nonlinear rotation overcomes the trap and the BEC ceases to exist. As a consequence of the density-dependent gauge potentials, the nonlinear rotation, $Cn(\mathbf{r}, t)$ gives rise to the density modulated angular velocity within the BEC. The different density regions in a BEC with density-dependent gauge potentials, therefore, experience different rotations depending on the nature of nonlinear rotation. Such effective nonlinear rotations in the BEC can be induced by employing laser beams with spatially varying intensities and carrying l units of orbital angular momenta. From an experimental point of view, one can employ Laguerre-Gaussian laser beams with cylindrically varying intensity profiles and $l = 1$, recently used in realizing spin-angular-momentum-coupled BECs [28]. Furthermore, the density-dependent rotation in Eq. (10) is the combined (rigid-body and nonlinear) rotation, and the second gauged rotation still exists even when the externally driven rotation is absent ($\Omega_0 = 0$). The larger the number of atoms in a BEC, the easier it is to induce the nonlinear rotation and, therefore, the nucleation of the vortices in the BEC.

By expressing $\Psi(\mathbf{r}, t) = \psi(\boldsymbol{\rho}, t)\exp(-z^2/2\sigma_z^2)/\sqrt[4]{\pi\sigma_z^2}$ for a BEC of thickness σ_z confined in a highly anisotropic trap with $\omega_z \gg \omega_{x,y}$, and following the usual procedure of dimensional reduction [50], Eq. (9) results in the following two-dimensional (2D) GP equation:

$$i\hbar\frac{\partial\psi}{\partial t} = \left[-\frac{\hbar^2}{2m}\nabla_{\boldsymbol{\rho}}^2 + V(\boldsymbol{\rho}) - \Omega_n(\boldsymbol{\rho}, t)\hat{L}_z + g|\psi|^2 \right] \psi \quad (11)$$

The BEC, because of the high anisotropy and the absence of axial modes in case of sufficiently weak interactions [51], assumes a pancake geometry such that $\boldsymbol{\rho} = (x, y)$ represents the position vector in xy plane.

In quasi-2D settings, the operator $\nabla_{\boldsymbol{\rho}}^2 = \frac{\partial^2}{\partial x^2} + \frac{\partial^2}{\partial y^2}$, $V(\boldsymbol{\rho}) = \frac{1}{2}m(\omega_x^2 x^2 + \omega_y^2 y^2)$ is the 2D harmonic trapping potential, and the nonlinear coefficient, $g = g_{\text{eff}}/\sqrt{2\pi}\sigma_z$. The density-dependent trap rotation $\Omega_n(\boldsymbol{\rho}, t)$ has the same form as that in Eq. (10) except that C is now scaled by a factor of $1/\sqrt{2\pi}\sigma_z$ and $n(\boldsymbol{\rho}, t) = |\psi|^2$ is the 2D density of the BEC. In an elliptical trap with $\omega_{\perp}^2 = (\omega_x^2 + \omega_y^2)/2$ as the transverse trapping frequency, we assume $\omega_x = \omega_{\perp}\sqrt{1 - \epsilon}$ and $\omega_y = \omega_{\perp}\sqrt{1 + \epsilon}$ such that $\epsilon = (\omega_x^2 - \omega_y^2)/(\omega_x^2 + \omega_y^2)$ determines the trap ellipticity. This ellipticity in the trapping potential breaks the rotational symmetry which is crucial for the nucleation of vortices in BECs. By means of spatiotemporal scaling [45, 52], $t = \omega_{\perp}^{-1}t'$, $(x, y) = a_{\perp}(x', y')$, and $\psi = \frac{\sqrt{N}}{a_{\perp}}\psi'$, Eq. (11) can be recast in the following normalized form:

$$(i - \gamma)\frac{\partial\psi}{\partial t} = \left[-\frac{\nabla_{\boldsymbol{\rho}}^2}{2} + V(\boldsymbol{\rho}) - \tilde{\Omega}_n(\boldsymbol{\rho}, t)\hat{L}_z + \tilde{g}|\psi|^2 \right] \psi. \quad (12)$$

In Eq. (12), the scaled parameters, $\tilde{g} = gNm/\hbar^2$ and $\tilde{\Omega}_n(\boldsymbol{\rho}, t) = \Omega_0/\omega_{\perp} + \tilde{C}n(\boldsymbol{\rho}, t)$, where $\tilde{C} = CNm/(\hbar\sqrt{2\pi}\sigma_z)$. In this dimensionless form the 2D wavefunction $\psi(\boldsymbol{\rho}, t)$ is now normalized to unity, the elliptical trapping potential, $V(\boldsymbol{\rho}) = \frac{1}{2}[(1 - \epsilon)x^2 + (1 + \epsilon)y^2]$ and $\hat{L}_z = -i(x\frac{\partial}{\partial y} - y\frac{\partial}{\partial x})$ is the angular-momentum operator. The term γ is introduced to account for any dissipation in the system [53]. By setting $\gamma = 0.03$ [43–45, 54] and $\omega_{\perp} = 2\pi \times 200$ Hz in the following, we study the effects of density-dependent gauge potentials on the dynamics of vortex nucleation in a harmonically confined BEC by directly solving the generalised GP equation (12) numerically. The dissipation term fastens the convergence to the equilibrium state characterized by a vortex-lattice and does not affect the dynamics of the BEC.

III. NUMERICAL ANALYSIS

The introduction of trap rotation, Ω_0 and anisotropy, ϵ have been employed both experimentally [2, 3] and numerically [18, 44, 45] to evolve the harmonically confined BECs for the nucleation of vortices. In either case, the BEC is first deformed to an elliptical cloud, undergoes shape oscillations and is subsequently nucleated with vortices. The deformation of the condensate due to the trap rotation is parameterized by the factor $\alpha_0 = \Omega_0(\langle x^2 - y^2 \rangle / \langle x^2 + y^2 \rangle)$ with $\langle \dots \rangle$ representing the expectation values and was first obtained theoretically by Recati *et al.* [6] by employing a hydrodynamic formulation [6, 7]. In this formalism the value of α_0 in units of ω_{\perp} satisfies the cubic equation, $\alpha_0^3 + (1 + 2\Omega_0/\omega_{\perp})\alpha_0 - \epsilon\Omega_0/\omega_{\perp} = 0$, whose solutions for a given free parameter (Ω_0 or ϵ), form branches that mark the routes toward the instability in the respective parameter space. The free parameter (Ω_0 or ϵ) is varied adiabatically until either a dynamical instability is reached or the α branch back-bends [3, 6, 22]. For

$\alpha_0 > 0$, the BEC system is always dynamically unstable; otherwise the instability is caused by the branch back-bending. In the current scenario, the spatial dependence of the rotation complicates the hydrodynamic formulation. The phase profile of a rotating density-dependent BEC now also depends locally on the density distribution within the BEC. We, therefore, study the effects of density-dependent gauge potentials on the BEC deformation (α) and vortex nucleation in a harmonically trapped 2D BEC by employing the split-step Crank Nicholson method [55]. The modifications in the effective mean-field coupling constant due to the gauge potential are neglected.

An initial state for $\tilde{g} = 420$ and $\tilde{C} = 0, \pm 5$ is simulated via imaginary time propagation such that $\Delta x = 0.05$ and $\Delta t = 0.001$ are the space and time steps respectively. The initially simulated ground state is then followed in real time by ramping up either Ω_0 or ϵ linearly in time, thereby marking different routes for nucleation of vortices. The experimental tuning of interaction parameters, \tilde{g} and \tilde{C} through Feshbach resonances [56, 57] also paves way for controlling the dynamics of the respective condensate in the α - Ω_0 and α - ϵ parameter spaces. In any case, the number of atoms in the BEC is conserved by fixing the chemical potential after every time step. Moreover, the results remain unchanged for a ground state simulated with $\tilde{C} = 0$, followed by introducing Ω_0 or ϵ ramp and the nonlinear rotation simultaneously in real time.

We first consider the adiabatic increase of trap rotation frequency by making it time-dependent, $\Omega_0(t) = ft$ for $f \approx 1.6 \times 10^{-3} \omega_\perp^2$ and $\epsilon = 0.025$. The effect of the density-dependent gauge potentials on the deformation of the BEC is taken into account by defining,

$$\alpha = \frac{\langle \tilde{\Omega}_n(\boldsymbol{\rho}, t)(x^2 - y^2) \rangle}{\langle x^2 + y^2 \rangle} \quad (13)$$

for $\tilde{\Omega}_n(\boldsymbol{\rho}, t) = \Omega_0/\omega_\perp + \tilde{C}|\psi(\boldsymbol{\rho}, t)|^2$ and keeping the different parameter values same as mentioned in Ref. [2]. The expressions $\langle \dots \rangle$ in Eq. (13) represent the expectation values and hence α represents the net average deformation experienced by the density-dependent BEC. As the rotation frequency, Ω_0 is ramped up from zero, and the condensate follows the left branch for α (See Fig 1(a)), except for the small discrepancy due to its non-Thomas-Fermi nature, and becomes increasingly elongated as it goes through the higher values of α . Once Ω_{cr} is reached, the elongation in the BEC is maximum and the nucleated vortices at the surface start entering the condensate because of dynamical instability [7, 18]. The nucleated condensate finally returns to an axis-symmetric state specified by the drop in the α values. In Fig. 1 it is clear that the critical frequency values shift with the nature and strength of nonlinear rotation, \tilde{C} . For $\tilde{C} = \pm 5$, the critical frequencies are found to change by $\Delta\Omega_{cr} \approx \mp 0.02\omega_\perp$ respectively against the value of $\Omega_{cr} \simeq 0.74\omega_\perp$ for $\tilde{C} = 0$. In addition to shifting the critical frequency, the nonlinear rotation is seen to alter

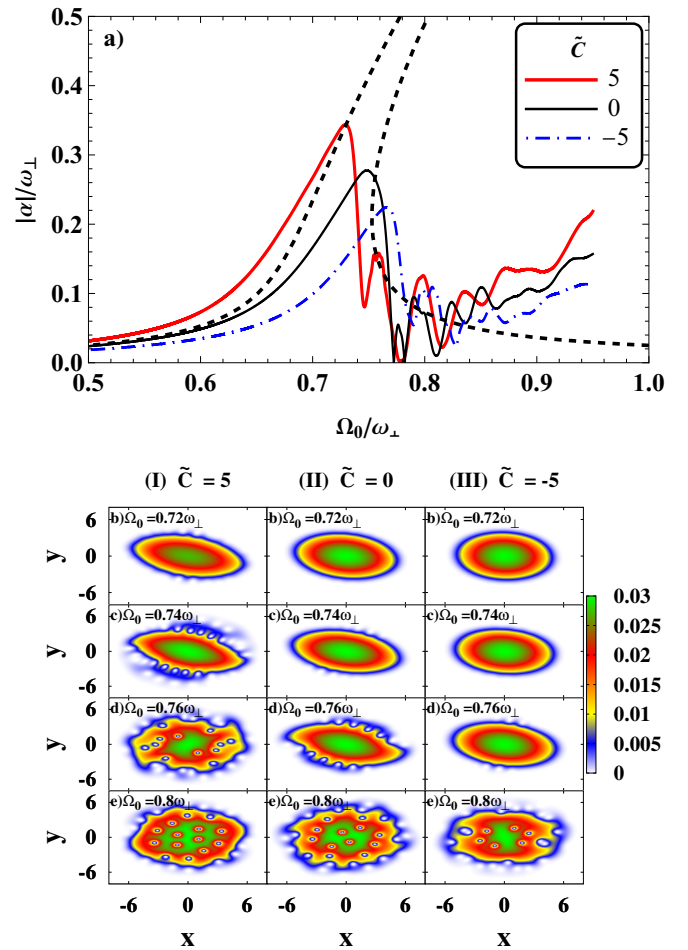


FIG. 1: (a) Time development of $|\alpha|/\omega_\perp$ for an ascending trap frequency, $\Omega_0(t)$ and $\epsilon = (\omega_x^2 - \omega_y^2)/(\omega_x^2 + \omega_y^2) = 0.025$. The color coded curves describe the numerical result for $\tilde{C} = CNm/(\hbar\sqrt{2\pi}\sigma_z) = 5, 0$ and -5 respectively while the black dashed curves describe the analytical result for $\tilde{C} = 0$ [6, 7]. The discrepancy between the analytical and numerical results for $\tilde{C} = 0$ correspond to the deviation of the density profile from the Thomas-Fermi limit. Columns I, II and III represent the time evolution of condensate density with $\tilde{C} = 5, 0$, and -5 respectively.

the values of α such that the condensates with larger \tilde{C} values are more elongated while following the left branch. This is directly linked with the number of the nucleated vortices within the condensate and hence, angular momentum. Consequently, the BECs with $\tilde{C} > 0$ are densely populated with the vortices and have large angular momentum values compared to the ones with $\tilde{C} < 0$ where the vortices mostly lie toward the periphery. This occurs due to the different rotations and hence energies ($E = E_0 - \tilde{\Omega}_n(\boldsymbol{\rho})L_z$) associated with the varying condensate densities. The BECs with $\tilde{C} > 0$ have their lowest energy regions at the center and hence get populated with vortices profusely. On the other hand, density-dependent BECs with $\tilde{C} < 0$ have their lowest energy zones at the periphery, thereby populating the vortices around the

condensate outskirts. The values of critical frequency, Ω_{cr} and the maximum condensate deformity, $|\alpha_{max}|$ in units of ω_{\perp} for the corresponding values of \tilde{C} are shown in Fig. 2. It is clear that the shifts in critical frequency

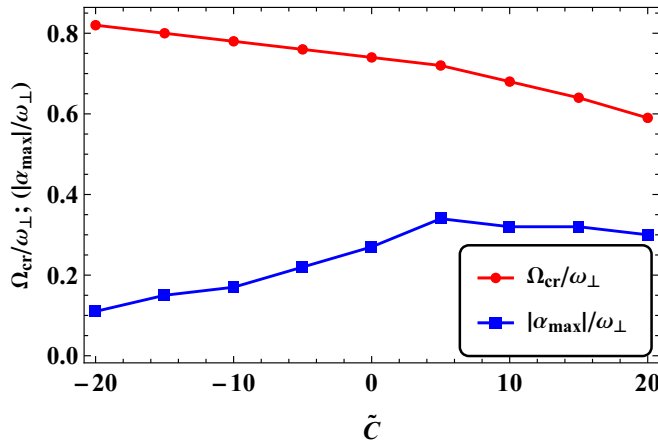


FIG. 2: Variation of the critical frequency, Ω_{cr} , and maximum deformation, $|\alpha_{max}|$ with the strength of nonlinear rotation, $\tilde{C} = CNm/(\hbar\sqrt{2\pi}\sigma_z)$ in a harmonically confined BEC with $\tilde{g} = 420$.

vary linearly with \tilde{C} for $\tilde{C} < 0$ and small $\tilde{C} > 0$ values. For large $\tilde{C} > 0$, the deviation from the linear behavior can be attributed to the non-Thomas-Fermi profiles of the corresponding BECs. In an analogous manner, the maximum condensate deformations, $|\alpha_{max}|$ corresponding to the Ω_{cr} values increase with increasing \tilde{C} and show anomaly for large values of $\tilde{C} > 0$.

Next, we consider the adiabatic increase in trap anisotropy by allowing ϵ to ramp up linearly from 0 to 0.025 at a rate $d\epsilon/dt \approx 6.2 \times 10^{-5}\omega_{\perp}$ for a fixed trap rotation frequency, Ω_0 . Like in the case of Ω_0 ramp, the BEC follows the respective α branch until the vortices start nucleating within the BEC at $\epsilon = \epsilon_{cr}$. In the ENS experiment involving an ϵ ramp [3], the nucleation of vortices in BECs with $\tilde{C} = 0$ was observed only if $\Omega_0 > \omega_{\perp}/\sqrt{2}$ whence the α branch shows back-bending. However, for $\Omega_0 < \omega_{\perp}/\sqrt{2}$, α is a monotonic function of ϵ and the numerical simulations [18] suggest that vortex nucleation can occur at a larger ϵ due to ripple instability. Since the net rotation and deformation experienced by the BEC is altered by the presence of density-dependent gauge potentials. Therefore, for a given Ω_0 , the nature of nonlinear rotation determines the branch followed by the BEC in α - ϵ space such that for large values of $\tilde{C} > 0$, the α branches exhibit back-bending even if $\Omega_0 < \omega_{\perp}/\sqrt{2}$. Similarly with $\Omega_0 \geq \omega_{\perp}/\sqrt{2}$, the α branches show no back-bending for large magnitudes of $\tilde{C} < 0$. Consequently, this regulates the values of ϵ_{cr} for vortex nucleation. Figures 3 and 4 show that for a BEC with given value of \tilde{C} and following an α branch without (with) back-bending, ϵ_{cr} decreases (increases) with the increase of the trap frequency. A similar effect due by the nonlinear rotation is inferred such that

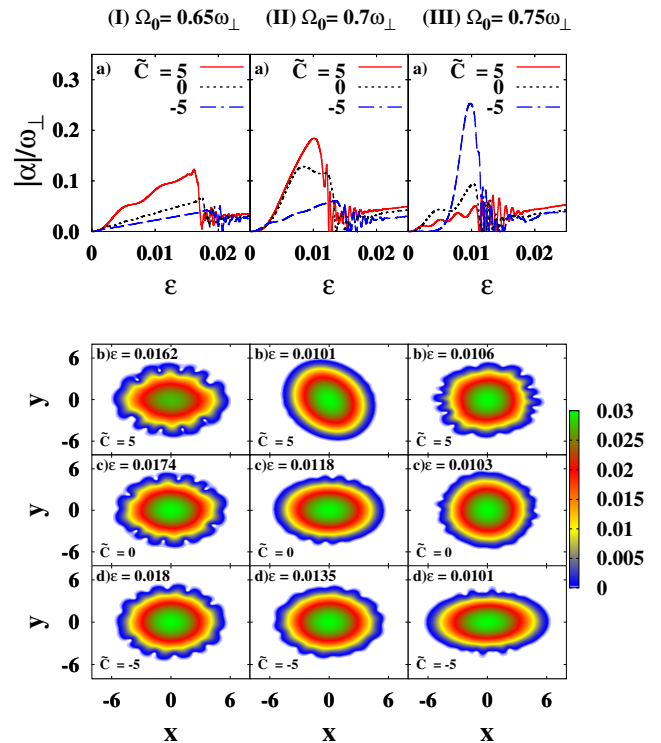


FIG. 3: (a) Time development of $|\alpha|/\omega_{\perp}$ for an ascending trap anisotropy, $\epsilon(t)$ at fixed Ω_0 values. For $\Omega_0/\omega_{\perp} = 0.65, 0.7, 0.75$, columns I (b)-(d), II (b)-(d) and III (b)-(d) respectively represent the density profiles at mentioned ϵ_{cr} and \tilde{C} values.

$\epsilon_{cr}(C > 0) < \epsilon_{cr}(C = 0) < \epsilon_{cr}(C < 0)$ for a given value of Ω_0 and the BEC follows an α branch without back-bending. The numerically obtained ϵ_{cr} values as a function of Ω_0 and \tilde{C} as well as the nature of the α branch followed by the BEC during an ϵ ramp are presented in Fig. 4 whereby it is evident that for an α branch without back-bending, the ϵ_{cr} values decrease with \tilde{C} values for fixed Ω_0 . However, for a BEC following an α branch with back-bending, ϵ_{cr} increases with \tilde{C} at a given value of Ω_0 . This is due to the drastic change in the BEC deformation by the presence of density-dependent gauge potentials and it depends on which side of $\omega_{\perp}/\sqrt{2}$, Ω_0 lies. For $\Omega_0 < \omega_{\perp}/\sqrt{2}$, the condensate deformation, α , decreases together with \tilde{C} while the situation is reversed with $\Omega_0 > \omega_{\perp}/\sqrt{2}$, where the condensate deformation increases with decreasing \tilde{C} values. This is nonetheless true for a narrow range of \tilde{C} values and anomalies occur at larger magnitudes. In an ϵ ramp, the vortex nucleation in BECs with $C = 0$ is shown to occur either by ripple, interbranch or catastrophic instability mechanisms, depending on the value of Ω_0 with respect to $\omega_{\perp}/\sqrt{2}$ [18]. In case of interbranch and catastrophic instability mechanisms, the respective α branches show back-bending in the α - ϵ parameter space. However, the back-bending of the α branch in catastrophic instability occurs at a larger ϵ compared to that of the interbranch instability.

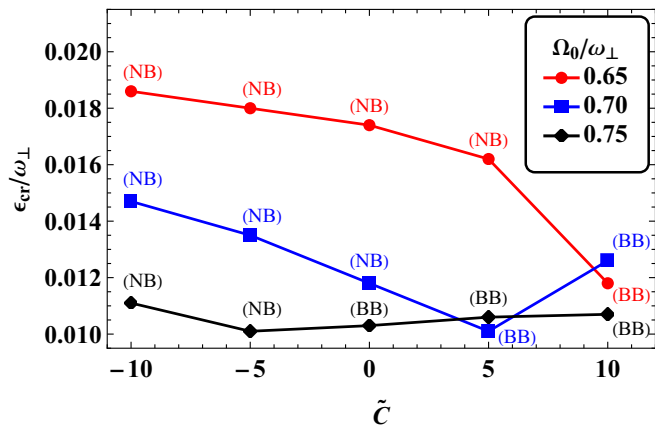


FIG. 4: Variation of ϵ_{cr} for corresponding values of Ω_0 and $\tilde{C} = CNm/(\hbar\sqrt{2\pi}\sigma_z)$ in a BEC with $\tilde{g} = 420$ and following an α branch with (BB) or without (NB) back-bending.

Though the nature of the α branch followed by the BEC during an ϵ ramp is modified by nonlinear rotation. However, in our numerical simulations, we did not observe the interbranch and catastrophic instability mechanisms and hence the role of \tilde{C} in tuning these mechanisms for vortex nucleation. As shown in Fig. 3, the vortex nucleation in all cases is due to the generation of ripples at the condensate surface rather than due to the shedding of low-density areas and contortion in interbranch and catastrophic instability mechanisms respectively.

So far we have focused on the response of the BEC with density-dependent gauge potentials to the slow turn on of the rotation of the trapping potential. We now consider the response of the BEC with the above set parameters against the sudden turn on of the rotation of the trap. When a BEC is rotated suddenly, it undergoes damped shape oscillations and ultimately relaxes into a state with vortex-lattice [2, 44]. As shown in Fig. 5, the nonlinear rotation has a prominent effect on these shape oscillations and thereby on the vortex nucleation, vortex dynamics and vortex-lattice formation. The shape oscillations become aperiodic and their amplitude increases for increasing $\tilde{C} > 0$. On the other hand, the amplitude and time period of the shape oscillations decreases with decreasing $\tilde{C} < 0$ as shown in Fig. 5(a). The nature of the vortex ground states and their achieving times are controlled by the nature and strength of nonlinear rotation, \tilde{C} . For $\tilde{C} = 5$, the vortex ground state is achieved at short times and the corresponding density profiles show that the BEC relaxes from the point of maximum elongation by shedding low-density material in a spiral pattern—*fragmentation* [58]. Consequently, surface waves and ghost vortices are generated which induce vortex nucleation. The vortices in the ground state, as shown in Fig. 5(I)(e), crystallize into a non-Abrikosov lattice which lack the hexagonal symmetry in the vortex arrangements. The BEC becomes disordered for large values of $\tilde{C} > 0$. In case $\tilde{C} = 0$, perfect triangular lattices, as shown in Fig. 5(II)(e), are obtained while the

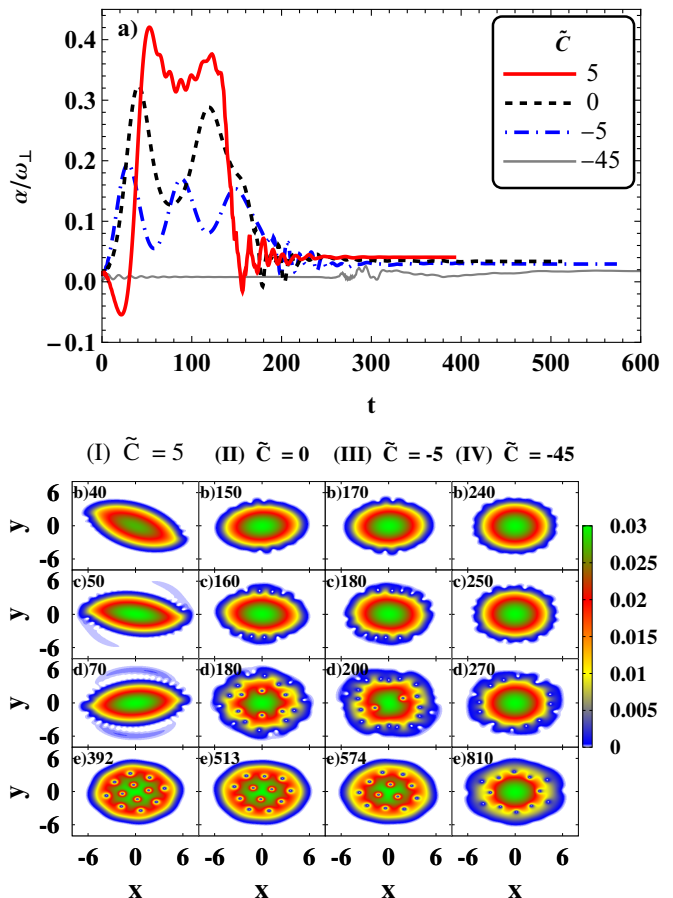


FIG. 5: (a) Time development of α/ω_{\perp} for different strengths of nonlinear rotation, \tilde{C} in a BEC suddenly rotated with $\Omega_0 = \omega_{\perp}/\sqrt{2}$. In the same scenario with $\tilde{g} = 420$, columns I-IV for $\tilde{C} = 5, 0, -5, -45$ respectively represent the time development of the BEC density.

non-Abrikosov vortex pattern again occurs for small values of $\tilde{C} < 0$. The ring-vortex arrangements, shown in Fig. 5(IV)(e), are obtained for large values of $\tilde{C} < 0$. Moreover, the vortex nucleation in BECs with $\tilde{C} \leq 0$ occurs through ripples rather than shedding of low density regions in BECs with $\tilde{C} > 0$. In deformed BECs, the excitations occur on the surfaces with less curvature. Since the BEC deformation decreases together with \tilde{C} , the condensates with large values of $\tilde{C} < 0$ are much symmetric and excitations occur uniformly throughout the surface as shown in Figs. 5(IV)(b) and 5(IV)(c). With regard to the effect on the number of vortices in the equilibrium states due by the nonlinear rotation, Fig. 6 displays the variation of the number of vortices with the strength of nonlinear rotation, \tilde{C} for given values of Ω_0 . In the vicinity of $\Omega_0 = \omega_{\perp}/\sqrt{2}$, the number of vortices do not change for a larger domain of \tilde{C} values, suggesting that the number of vortices in a suddenly rotated density-dependent BEC is fixed by the interaction strength, g , trap ellipticity, ϵ , and rotation frequency, Ω_0 , while non-

linear rotation, $\tilde{C}n(\boldsymbol{\rho}, t)$ only manipulates the position of the vortices within the condensate. However, this is not true for all trap rotation frequencies and the number of vortices also change on either side of $\tilde{C} = 0$. Except at high trap rotations, the number of vortices change in multiples of two and is attributed to the twofold symmetry of the trapping potential.

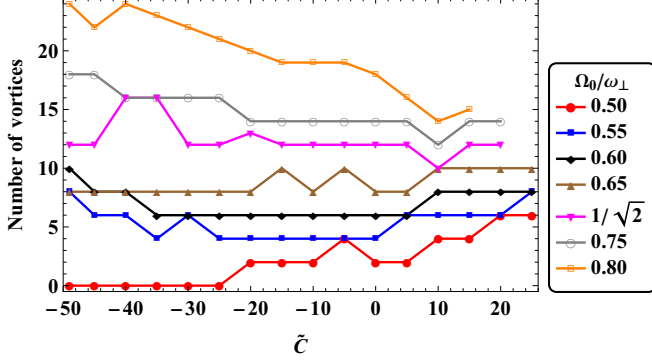


FIG. 6: Variation of the number of vortices with $\tilde{C} = CNm/(\hbar\sqrt{2\pi}\sigma_z)$ for fixed values of Ω_0 in a BEC with $\tilde{g} = 420$ and confined in an elliptical potential, $V(\mathbf{r}) = [(1-\epsilon)x^2 + (1+\epsilon)y^2]/2$ with $\epsilon = (\omega_x^2 - \omega_y^2)/(\omega_x^2 + \omega_y^2) = 0.025$

Further, it is worth mentioning that the vortex nucleation due to nonlinear rotation alone ($\Omega_0 = 0$) is anticipated for a BEC with large number of atoms [46, 48]. Our numerical experiments along this line shown in Fig. 7 displays that the average angular momentum, $\langle L_z \rangle = \langle \psi | i(y\partial/\partial x - x\partial/\partial y) | \psi \rangle$ values are still very small to ensure the formation of vortices within the BEC even for the mean-field interactions as large as, $\tilde{g} = 10000$. Nevertheless, $\langle L_z \rangle$ increases with \tilde{C} and \tilde{g} .

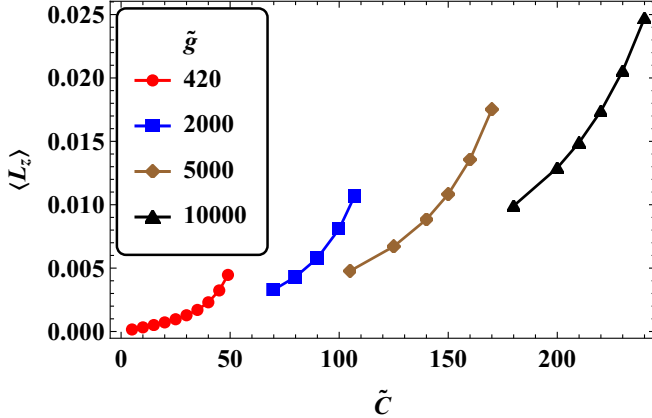


FIG. 7: Variation of $\langle L_z \rangle$ with \tilde{C} in the equilibrium states of the BEC for different strengths of \tilde{g} and no external trap rotation, $\Omega_0 = 0$. The topmost data point corresponds to a value closer to \tilde{C}_{\max} for the respective case.

We further examined the critical frequencies and the related single vortex dynamics by suddenly rotating the density-dependent BEC with $\tilde{g} = 420$ in a harmonic trap

displaced by $x_0 = 0.3a_\perp$ [59]:

$$V(\boldsymbol{\rho}) = \frac{1}{2} \left((x - x_0)^2 + y^2 \right) \quad (14)$$

The critical frequencies in units of ω_\perp are found to be 0.443, 0.461, and 0.47 for $\tilde{C} = 5, 0,$ and -5 respectively. These results are in accordance with the already mentioned results, though the BEC in this case deviates much from its stationary state because of sudden rotation. The single vortex nucleated at the boundary of the BEC traverses a spiral path before settling down at the minimum of the trap. Because of the density-dependent gauge potentials, the single vortex for a fixed trap rotation follows different trajectories depending on the nature of nonlinear rotation. The effect of nonlinear rotation strengths on the trajectory of a single vortex is presented in Fig. 8, where vortex positions and its distance from the trap center, $|\mathbf{R}_v|$ are traced at different instants of time. For fixed $\Omega_0 = 0.475\omega_\perp$, the single vortex first enters in BEC with $\tilde{C} > 0$, followed by the ones with $\tilde{C} = 0,$ and -5

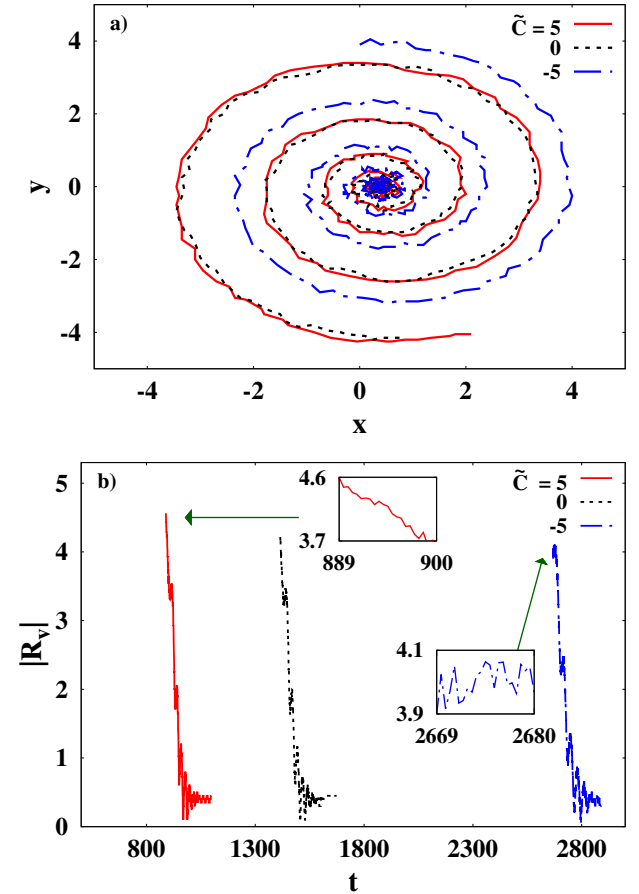


FIG. 8: (a) Single vortex trajectories in BECs with $\tilde{g} = 420$, $\tilde{C} = 0, \pm 5$ and rotated with $\Omega_0 = 0.475\omega_\perp$ in xy -coordinate space. (b) Time evolution of vortex position in terms of its radial distance $|\mathbf{R}_v|$ from the trap center. The vortex finally sits around the trap minimum at $(x_0, y_0) = (0.3, 0.0)a_\perp$

respectively. The first appearances of the vortex in the BECs with $\tilde{C} = 5, 0, -5$ were at $|\mathbf{R}_v|(a_\perp) \approx 4.6, 4.2, 3.9$. This is due to the larger net rotation and the associated size in case of BECs with $\tilde{C} > 0$. Moreover, in density-dependent BECs, the Magnus force, $\mathbf{f} = n(\boldsymbol{\rho}, t)\mathbf{K} \times \mathbf{v}$ for a given density distribution, $n(\boldsymbol{\rho}, t)$, circulation, \mathbf{K} and vortex velocity, $\mathbf{v} = -y\tilde{\Omega}_n(\boldsymbol{\rho}, t)\hat{e}_x + x\tilde{\Omega}_n(\boldsymbol{\rho}, t)\hat{e}_y$ is modified by the nonlinear rotation. In fact, the vorticity, $\omega = [2\tilde{\Omega}_n(\boldsymbol{\rho}, t) + \tilde{C}(x\partial n(\boldsymbol{\rho}, t)/\partial x + y\partial n(\boldsymbol{\rho}, t)/\partial y)]\hat{e}_z$ is now a function of both space and time. The result is that in case of harmonically confined density-dependent BECs with $\tilde{C} > 0$, the Magnus force is enhanced radially inwards and thereby the vortex moves swiftly toward the trap center, as confirmed in inset of Fig. 8(b). This is contrary to the case when $\tilde{C} < 0$ where the Magnus force is reduced by the nonlinear rotation and hence the vortex moves slowly toward the trap center, as shown by the corresponding inset in Fig. 8(b). The vortex stays at the boundary for long before getting within the bulk of the condensate. The time taken in units of ω_\perp by the single vortex to reach the minimum of the trap is found to be $\approx 115, 186$ and 221 respectively for $\tilde{C} = 5, 0$ and -5 . For large negative values of \tilde{C} , the Magnus force is outbalanced and the vortices reside at the fast rotating periphery, thereby favoring ring-vortex arrangements.

The formation of ring-vortex arrangements is further supported by the presence of modified repulsive interactions between the vortices within the BEC. In this direction we simulated the equilibrium states with two and three vortices respectively. It is found that the separation between the vortices increases with the strength of $\tilde{C} < 0$ as shown in Fig. 9. For $\tilde{C} > 0$, the vor-

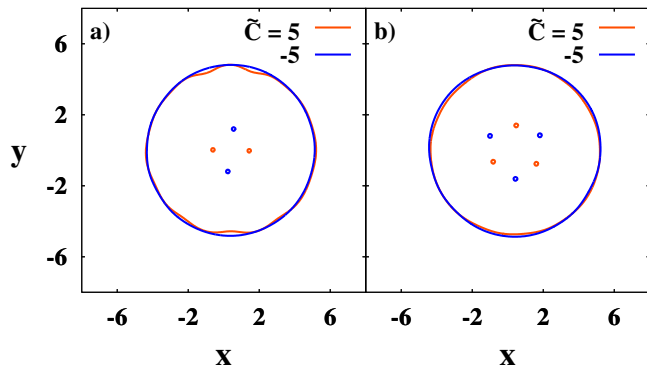


FIG. 9: Contour-plots showing vortices in density-dependent BEC with $\tilde{C} = \pm 5$ and rotated with (a) $\Omega_0 = 0.51\omega_\perp$ and (b) $\Omega_0 = 0.525\omega_\perp$ respectively. The respective results show same number of vortices with different positions for the same trap rotation frequency.

tices come closer, making their separation smaller than $\tilde{C} = 0$. Consequently, the strength of vortex-vortex repulsion decreases with the increase in the strength of nonlinear rotation and vice-versa. A condensate with the above set of values for the s -wave interactions when rotated at $\Omega_0 = 0.51\omega_\perp$ is nucleated with two vortices

as shown in Fig. 9(a). The separation in units of a_\perp between the two vortices for $\tilde{C} = 5$ and -5 are respectively found to be 2.05 and 2.41. These values correspond to an $\sim 8\%$ change in mean vortex separation with $\tilde{C} = 0$. The same results are inferred from the simulations of the ground states with three vortices shown in Fig. 9(b), where the area changes by $\sim 15\%$ from the mean value. The change in separation between the vortices can be qualitatively explained by considering the method of images [60]. This method estimates that the equilibrium separation between two neighboring vortices in a BEC is $d = \frac{1}{\sqrt{2\Omega_0/\omega_\perp}}$ as $\Omega_0 \rightarrow \omega_\perp$. Along similar lines, for a density-dependent BEC $d \propto \frac{1}{\sqrt{\tilde{\Omega}_n(\boldsymbol{\rho}, t)}}$ where

$\tilde{\Omega}_n(\boldsymbol{\rho}, t) = \Omega_0/\omega_\perp + \tilde{C}n(\boldsymbol{\rho}, t)$. This relation shows that the distance between vortices decreases (increases) with the increasing (decreasing) strength of nonlinear rotation as shown in Fig. 9. Moreover, for a fixed value of \tilde{C} the separation between the vortices will also depend on the density distribution of the BEC. For a given value of Ω_0 and $\tilde{C} > 0$ the vortices in the center will be closer to each other than the ones in the periphery of the BEC. However if $\tilde{C} < 0$, then the vortices in the center will be distant from each other and for large negative values of \tilde{C} , the vortices reside only in the periphery of the BEC. The modifications in the vortex-vortex separation by the density-dependent gauge potentials thus result in the formation of non-Abrikosov vortex lattices and ring-vortex arrangements. Consequently, the areal density of vortices within the stationary states of density-dependent BECs is nonuniform and is regulated by the density distribution of the BEC through nonlinear rotation. These modifications due by the nonlinear rotation have an additional effect on the number of vortices within the BEC. Figure 10 shows the variation of the number of vortices in the BEC trapped in a harmonic potential (14) with \tilde{C} for given values of Ω_0 . The results are consistent with those presented in Fig. 6, except that the change in the vortex number now can be even or odd.

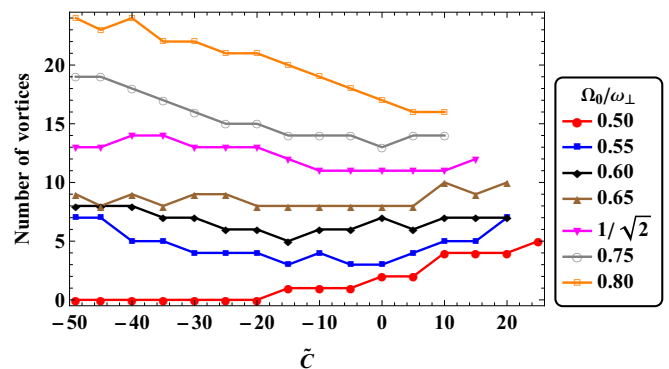


FIG. 10: Variation of the number of vortices with $\tilde{C} = CNm/(\hbar\sqrt{2\pi}\sigma_z)$ for fixed values of Ω_0 in a BEC with $\tilde{g} = 420$ and $V(\mathbf{r}) = ((x - x_0)^2 + y^2)/2$.

IV. CONCLUSIONS

In this work we consider a harmonically trapped 2D BEC subjected to a density-dependent gauge potential and theoretically studied the vortex nucleation in it by employing direct numerical simulations. The presence of density-dependent gauge potential realises nonlinear rotation in BECs. The nonlinear rotation alters the net rotation and deformation experienced by the BEC. This consequently shifts the critical frequencies, Ω_{cr} for the vortex nucleation. The shifts in the frequency values depend on the strength and nature of the nonlinear rotation. Consequently, the BECs with $C > 0$ experience an increased net rotation and their critical frequencies are lowered. However, in BECs with $C < 0$, the net rotation of the condensate is lowered while the critical frequencies soar higher. In general, for any BEC, the critical frequencies follow the order $\Omega_{\text{cr}}(C > 0) < \Omega_{\text{cr}}(C = 0) < \Omega_{\text{cr}}(C < 0)$. The critical frequencies for the transition to vortex-lattices in BECs with density-dependent gauge potentials, therefore, depend on the strength of the short range s -wave interactions within them, contrary to the conventional and dipolar BECs with $C = 0$. The nonlinear rotation due to the density-dependent gauge potential also determines the number and arrangement of vortices within the rotating BECs. Moreover, in nonuniform BECs subjected to density-dependent gauge potentials, different density regions experience different rotations. This has a direct impact on the motion of the vortices within the condensate. In comparison to the BECs with $C \leq 0$, it is found that a single vortex in BECs with $C > 0$ moves swiftly and takes less time to reach the trap center when the system attains equilibrium. The Magnus force on the vortices is expected to get modified for the cause. Moreover, the mutual repulsive interactions between the vortices in a multiple vortex system are also modified by the presence of density-dependent gauge potentials. The distance between the vortices and

their areal density now depends on the density distribution of the BEC and the strength and sign of nonlinear rotation. The combined effects of these modified forces and the interactions along with energy considerations result in non-Abrikosov vortex-lattices and ring-vortex arrangements.

Like critical frequency, nonlinear rotation due to the density-dependent gauge potentials also regulate the critical ellipticity, ϵ_{cr} for vortex nucleation. At a fixed Ω_0 , the critical ellipticities follow the trend of critical frequencies *i.e.*, $\epsilon_{\text{cr}}(C > 0) < \epsilon_{\text{cr}}(C = 0) < \epsilon_{\text{cr}}(C < 0)$ in case the BEC follows an α branch without back-bending. However, the trend is reversed for a BEC following an α branch with back-bending.

It would be interesting to extend the present work by considering density-dependent BECs in optical lattices on top of the harmonic traps. In addition to the surface instability, vortex nucleation in conventional BECs with optical lattices even occurs through the generation of vortex-antivortex pairs in the bulk [61]. The pair generation occurs only if the lattice spacings are greater than the critical values. It is, therefore, natural to investigate the effects of density-dependent gauge potentials on the dynamics of vortex nucleation in such BEC systems. Moreover, the findings can be realized in experiments since the density-dependent gauge potentials have already been demonstrated in two-dimensional optical lattices [30, 31].

V. ACKNOWLEDGEMENTS

The authors thank P. G. Kevrekidis for fruitful discussions. B.D. thanks Science and Engineering Research Board, Government of India for funding through research project CRG/2020/003787. I.A.B. acknowledges CSIR, Government of India, for funding via CSIR Research Associateship (09/137(0627)/2020 EMR-I).

-
- [1] M. R. Matthews, B. P. Anderson, P. C. Haljan, D. S. Hall, C. E. Wieman, and E. A. Cornell, Phys. Rev. Lett. **83**, 2498 (1999).
 - [2] K. W. Madison, F. Chevy, W. Wohlleben, and J. Dalibard, Phys. Rev. Lett. **84**, 806 (2000).
 - [3] K. W. Madison, F. Chevy, V. Bretin, and J. Dalibard, Phys. Rev. Lett. **86**, 4443 (2001).
 - [4] E. Hodby, G. Hechenblaikner, S. A. Hopkins, O. M. Maragò, and C. J. Foot, Phys. Rev. Lett. **88**, 010405 (2001).
 - [5] J. R. Abo-Shaeer, C. Raman, J. M. Vogels, and W. Ketterle, Science **292**, 476 (2001).
 - [6] A. Recati, F. Zambelli, and S. Stringari, Phys. Rev. Lett. **86**, 377 (2001).
 - [7] S. Sinha and Y. Castin, Phys. Rev. Lett. **87**, 190402 (2001).
 - [8] R. J. Donnelly, Quantized Vortices in Helium II, vol. 2 (Cambridge University Press, Cambridge, UK, 1991).
 - [9] V. Yukalov, A. Novikov, E. Yukalova, and V. S. Bagnato, in Journal of Physics: Conference Series (IOP Publishing, Bristol, 2016), vol. 691, p. 012019.
 - [10] H. Middleton-Spencer, A. Orozco, L. Galantucci, M. Moreno, N. Parker, L. Machado, V. Bagnato, and C. Barenghi, arXiv:2204.08544 (2022).
 - [11] K. Sasaki, N. Suzuki, and H. Saito, Physical review letters **104**, 150404 (2010).
 - [12] W. J. Kwon, G. Moon, S. W. Seo, and Y.-i. Shin, Physical Review A **91**, 053615 (2015).
 - [13] A. L. Fetter, Rev. Mod. Phys. **81**, 647 (2009).
 - [14] F. Dalfovo, S. Giorgini, L. P. Pitaevskii, and S. Stringari, Rev. Mod. Phys. **71**, 463 (1999).
 - [15] T. K. Ghosh, Phys. Rev. A **69**, 043606 (2004).
 - [16] T. Mithun, K. Porsezian, and B. Dey, Phys. Rev. E **88**, 012904 (2013).
 - [17] F. Chevy, K. W. Madison, and J. Dalibard, Phys. Rev. Lett. **85**, 2223 (2000).

- [18] N. G. Parker, R. M. W. van Bijnen, and A. M. Martin, *Phys. Rev. A* **73**, 061603 (2006).
- [19] Y. Cai, Y. Yuan, M. Rosenkranz, H. Pu, and W. Bao, *Phys. Rev. A* **98**, 023610 (2018).
- [20] D. H. J. O'Dell and C. Eberlein, *Phys. Rev. A* **75**, 013604 (2007).
- [21] R. M. W. van Bijnen, D. H. J. O'Dell, N. G. Parker, and A. M. Martin, *Phys. Rev. Lett.* **98**, 150401 (2007).
- [22] R. M. W. van Bijnen, A. J. Dow, D. H. J. O'Dell, N. G. Parker, and A. M. Martin, *Phys. Rev. A* **80**, 033617 (2009).
- [23] S. B. Prasad, T. Bland, B. C. Mulkerin, N. G. Parker, and A. M. Martin, *Phys. Rev. Lett.* **122**, 050401 (2019).
- [24] J. Dalibard, F. Gerbier, G. Juzeliūnas, and P. Öhberg, *Reviews of Modern Physics* **83**, 1523 (2011).
- [25] N. Goldman, G. Juzeliūnas, P. Öhberg, and I. B. Spielman, *Reports on Progress in Physics* **77**, 126401 (2014).
- [26] M. J. Edmonds, M. Valiente, G. Juzeliūnas, L. Santos, and P. Öhberg, *Phys. Rev. Lett.* **110**, 085301 (2013).
- [27] Y.-J. Lin, K. Jiménez-García, and I. B. Spielman, *Nature* **471**, 83 (2011).
- [28] H.-R. Chen, K.-Y. Lin, P.-K. Chen, N.-C. Chiu, J.-B. Wang, C.-A. Chen, P. Huang, S.-K. Yip, Y. Kawaguchi, and Y.-J. Lin, *Phys. Rev. Lett.* **121**, 113204 (2018).
- [29] D. Zhang, T. Gao, P. Zou, L. Kong, R. Li, X. Shen, X.-L. Chen, S.-G. Peng, M. Zhan, H. Pu, et al., *Phys. Rev. Lett.* **122**, 110402 (2019).
- [30] L. W. Clark, B. M. Anderson, L. Feng, A. Gaj, K. Levin, and C. Chin, *Phys. Rev. Lett.* **121**, 030402 (2018).
- [31] F. Görg, K. Sandholzer, J. Minguzzi, R. Desbuquois, M. Messer, and T. Esslinger, *Nat. Phys.* **15**, 1161 (2019).
- [32] T. Keilmann, S. Lanzmich, I. McCulloch, and M. Roncaglia, *Nat. Commun.* **2**, 1 (2011).
- [33] U. Aglietti, L. Griguolo, R. Jackiw, S.-Y. Pi, and D. Semirara, *Phys. Rev. Lett.* **77**, 4406 (1996).
- [34] I. A. Bhat, S. Sivaprakasam, and B. A. Malomed, *Phys. Rev. E* **103**, 032206 (2021).
- [35] R. Dingwall, M. Edmonds, J. Helm, B. Malomed, and P. Öhberg, *New Journal of Physics* **20**, 043004 (2018).
- [36] R. Dingwall and P. Öhberg, *Physical Review A* **99**, 023609 (2019).
- [37] M. J. Edmonds, M. Valiente, and P. Öhberg, *EPL (Europhysics Letters)* **110**, 36004 (2015).
- [38] L. Chen and Q. Zhu, *New Journal of Physics* **24**, 053044 (2022).
- [39] M. Edmonds and M. Nitta, *Phys. Rev. A* **102**, 011303 (2020).
- [40] M. Edmonds, *Phys. Rev. A* **104**, 043310 (2021).
- [41] L. J. Campbell and R. M. Ziff, *Physical Review B* **20**, 1886 (1979).
- [42] T. Sato, T. Ishiyama, and T. Nikuni, *Physical Review A* **76**, 053628 (2007).
- [43] T. Mithun, K. Porsezian, and B. Dey, *Physical Review A* **93**, 013620 (2016).
- [44] M. Tsubota, K. Kasamatsu, and M. Ueda, *Phys. Rev. A* **65**, 023603 (2002).
- [45] K. Kasamatsu, M. Tsubota, and M. Ueda, *Phys. Rev. A* **67**, 033610 (2003).
- [46] S. Butera, M. Valiente, and P. Öhberg, *Journal of Physics B: Atomic, Molecular and Optical Physics* **49**, 015304 (2016).
- [47] S. Butera, M. Valiente, and P. Öhberg, *New Journal of Physics* **18**, 085001 (2016).
- [48] S. Butera, Ph.D. thesis, Heriot-Watt University (2017).
- [49] G. Juzeliūnas, P. Öhberg, J. Ruseckas, and A. Klein, *Physical Review A* **71**, 053614 (2005).
- [50] G. Yunyi, Master's thesis, National University of Singapore (2005).
- [51] D. S. Petrov, M. Holzmann, and G. V. Shlyapnikov, *Phys. Rev. Lett.* **84**, 2551 (2000).
- [52] V. M. Pérez-García, H. Michinel, and H. Herrero, *Phys. Rev. A* **57**, 3837 (1998).
- [53] S. Choi, S. Morgan, and K. Burnett, *Phys. Rev. A* **57**, 4057 (1998).
- [54] T. Mithun, K. Porsezian, and B. Dey, *Physical Review A* **89**, 053625 (2014).
- [55] P. Muruganandam and S. K. Adhikari, *Comput. Phys. Commun.* **180**, 1888 (2009).
- [56] S. Inouye, M. Andrews, J. Stenger, H.-J. Miesner, D. M. Stamper-Kurn, and W. Ketterle, *Nature* **392**, 151 (1998).
- [57] S. Blatt, T. Nicholson, B. Bloom, J. Williams, J. Thomsen, P. Julienne, and J. Ye, *Phys. Rev. Lett.* **107**, 073202 (2011).
- [58] N. G. Parker and C. S. Adams, *Phys. Rev. Lett.* **95**, 145301 (2005).
- [59] P. G. Kevrekidis, D. J. Frantzeskakis, and R. Carretero-González, *Emergent Nonlinear Phenomena in Bose-Einstein Condensates: Theory and Experiment*, vol. 45 (Springer, Berlin, 2008).
- [60] N. Verhelst and J. Tempere, in *Vortex Dynamics and Optical Vortices*, edited by H. Perez-De-Tejada (Vortex Dynamics. Intech, 2017), chap. 1.
- [61] A. Kato, Y. Nakano, K. Kasamatsu, and T. Matsui, *Phys. Rev. A* **84**, 053623 (2011).